Monthly Notices of the ROYAL ASTRONOMICAL SOCIETY
MNRAS **469**, 1521–1531 (2017) doi:10.1093/mnras/stx934
Advance Access publication 2017 April 19

The extended law of star formation: the combined role of gas and stars

Sami Dib,[1]★ Sacha Hony[2] and Guillermo Blanc[3,4,5]

[1] *Universidad de Atacama, Copayapu 485, Copiapó, Chile*
[2] *Institut für Theoretische Astrophysik, Zentrum für Astronomie der Universität Heidelberg, Albert-Überle-Straße 2, D-69120 Heidelberg, Germany*
[3] *Observatories of the Carnegie Institution for Science, 813 Santa Barbara St, Pasadena, CA, 91101, USA*
[4] *Departamento de Astronomía, Universidad de Chile, Camino del Observatorio 1515, Las Condes, Santiago, Chile*
[5] *Centro de Astrofísica y Tecnologías Afines (CATA), Camino del Observatorio 1515, Las Condes, Santiago, Chile*

Accepted 2017 April 13. Received 2017 April 11; in original form 2017 February 3

ABSTRACT

We present a model for the origin of the extended law of star formation in which the surface density of star formation ($\Sigma_{\rm SFR}$) depends not only on the local surface density of the gas ($\Sigma_{\rm g}$) but also on the stellar surface density (Σ_*), the velocity dispersion of the stars and on the scaling laws of turbulence in the gas. We compare our model with the spiral, face-on galaxy NGC 628 and show that the dependence of the star formation rate on the entire set of physical quantities for both gas and stars can help explain both the observed general trends in the $\Sigma_{\rm g} - \Sigma_{\rm SFR}$ and $\Sigma_* - \Sigma_{\rm SFR}$ relations, but also, and equally important, the scatter in these relations at any value of $\Sigma_{\rm g}$ and Σ_*. Our results point out to the crucial role played by existing stars along with the gaseous component in setting the conditions for large scale gravitational instabilities and star formation in galactic discs.

Key words: ISM: structure – galaxies: evolution – galaxies: ISM – galaxies: kinematics and dynamics – galaxies: star formation – galaxies: stellar content.

1 INTRODUCTION

The star formation rate (SFR) is the quantity that describes how galaxies convert their gas reservoirs into stars per unit time. Quantifying the dependence of the SFR on the global properties of galaxies as well as on the local conditions within galaxies is essential towards understanding their observed properties and their dynamical and chemical evolution across cosmic time. Traditionally, observational studies have sought the correlation between the surface density of star formation ($\Sigma_{\rm SFR}$) and the surface density of the gas $\Sigma_{\rm g} = \Sigma_{\rm H\,I} + \Sigma_{\rm H_2}$, where $\Sigma_{\rm H\,I}$ and $\Sigma_{\rm H_2}$ are the surface densities of the neutral and molecular hydrogen, respectively. The emerging picture from all of these works is that $\Sigma_{\rm SFR} \propto \Sigma_{\rm g}^n$ with $n \approx 1.4$ (e.g. Schmidt 1959; Kennicutt 1998; Bigiel et al. 2008; Blanc et al. 2009). Other studies found that the surface density of star formation scales linearly or sub-linearly ($n \lesssim 1$) with the surface density of molecular hydrogen traced by CO lines or with the surface density of molecules that trace higher density gas such as HCN (e.g. Gao & Solomon 2004; Shetty, Kelly & Bigiel 2013; Liu et al. 2016). Several ideas have been proposed in order to explain the origin of the star formation scaling relations. The earliest scenarios proposed that stars form as a result of gravitational instabilities (GIs) in the gaseous component of galactic discs over a time-scale, which is the local free-fall time of the gas and is given by $t_{\rm ff,g} \propto \rho_{\rm g}^{-0.5}$, where $\rho_{\rm g}$ is the local gas volume density. For a constant scaleheight of the disc, $\rho_{\rm g} \propto \Sigma_{\rm g}$ and thus $\Sigma_{\rm SFR} \propto \Sigma_{\rm g}/t_{\rm ff,g} \propto \Sigma_{\rm g}^{1.5}$ (e.g. Madore 1977). Wong & Blitz (2002) argued that the value of the star formation law slope is related to the value of the molecular fraction $f_{\rm H_2} = \Sigma_{\rm H_2}/\Sigma_{\rm g}$, and Blitz & Rosolowsky (2006) showed that $f_{\rm H_2}$ can be related to the pressure of the interstellar medium. It was also suggested that the value of n is related to the width of the density probability distribution function of the interstellar gas and to the threshold density that is associated with the gas tracer (Tassis 2007; Wada & Norman 2007). Escala (2011) argued that a correlation exists between the largest mass-scale for structures not stabilized by rotation and the SFR. Other groups (e.g. Krumholz & McKee 2005; Hennebelle & Chabrier 2011; Padoan & Nordlund 2011; Federrath 2013; Kraljic et al. 2014) explored ideas based on the role of turbulent fragmentation in giant molecular clouds (GMCs) and in which the SFR is a function of the dynamical properties of the clouds. Meidt et al. (2013) argued that the SFR in molecular clouds in M51 may correlate with the intensity of the dynamical pressure the clouds are subjected to. The role of feedback coupled to turbulent fragmentation and its effects on the regulation of the SFR on galactic scales have been included in a number of models (e.g. Dopita 1985; Dopita & Ryder 1994; Dib et al. 2011a, Dib et al. 2011b; Dib 2011a,b; Renaud, Kraljic & Bournaud 2012; Dib et al. 2013; Orr et al. 2017).

★ E-mail: sami.dib@gmail.com

It is however necessary to include stars in the treatment of GI on large scales in galactic discs, since in most disc galaxies, the stellar surface density is observed to be a factor ≈10–100 larger than the gas surface density (e.g. Leroy et al. 2008). The role of existing stars in determining the development of GIs has been investigated in a limited number of studies. Jog & Solomon (1984a,b) explored the characteristics of the GI in a two fluid medium (gas and stars) in which both components interact gravitationally with each other and are treated each as an isothermal gas with specific velocity dispersions. One of their main conclusions is that even when each fluid component is gravitationally stable, the joint fluid system may be gravitationally unstable. Rafikov (2001) expanded the study of Jog & Solomon to the case where the stars are treated as a collisionless component. Setting stars aside, Romeo, Burkert & Agertz (2010) investigated the role of turbulent motions on the stability of galactic discs. They described interstellar turbulence using scaling laws that relate the size of a region to the gas surface density (Σ_g) and gas velocity dispersion (σ_g). Romeo & Agertz (2014) investigated the development of GI for various regimes of turbulence (i.e. different dependence of Σ_g and Σ_g on the physical scale). In parallel, Romeo & Wiegert (2011) and Romeo & Falstad (2013) proposed a derivation of the effective Toomre Q parameter (Toomre 1964) for multicomponent discs of stars and gas and taking into account the effects of disc thickness. Shadmehri & Khajenabi (2012) and Hoffman & Romeo (2012) coupled aspects of the analysis of Jog & Solomon (1984a) to that of Romeo et al. (2010) and investigated the linear growth rate of the GI in a gas+star galactic disc while at the same time accounting for the turbulent nature of the gas. On the observational side, Shi et al. (2011) showed that the scatter in the Σ_g–Σ_{SFR} relation may be reduced if Σ_{SFR} is a function that depends on both Σ_g and Σ_*. When describing Σ_{SFR} as the product of two power-law functions of the gas and stellar surface densities ($\Sigma_{SFR} \propto \Sigma_g^{\alpha}\, \Sigma_*^{\beta}$). They obtained $\alpha = 0.8 \pm 0.01$ and $\beta = 0.63 \pm 0.01$ from the combined measurements on sub-galactic scales (scales of ≈750 pc) of 12 nearby galaxies, with a non-negligible galaxy-to-galaxy scatter when the data of each galaxy is fitted individually (see also Westfall et al. 2014). Rahmani, Lianou & Barmby (2016) performed a similar study for the Andromeda galaxy, and showed that these exponents may well depend on the distance from the centre of the galaxy. It is important to mention that the description of the extended law of star formation as being the product of two power laws (for gas and stars) is an empirical one, and possibly is an over-simplification of the physical processes that may be connecting the gas and stellar properties to the SFR.

However, in all of these above mentioned works, the origin of the dependence of the surface density of star formation on the local properties of the gas and stars has not been explicitly quantified. In this work, we examine the role of GI in a two fluid medium (gas and stars) and investigate the quantitative relationship between the surface density of the SFR and the surface densities and velocity dispersions of the stellar and turbulent gaseous components.[1] The basis of our model is that the fastest growing mode of the GI is the one that is directly connected to the SFR. In Section 2, we recall the basic equations that lead to the derivation of the wavelength of the fastest growing mode in a stellar+turbulent gas disc (λ_{SF}), and to the quantitative dependence of Σ_{SFR} on λ_{SF} and other gas and stellar structural and dynamical properties. In Section 3, we make a detailed comparison between the predictions of the Σ_{SFR} from our model and the observed values for the face-own, spiral galaxy NGC 628. We also discuss how including the effects of stellar feedback can affect, and in fact improve, the matching between the models and the observations. In Section 4, we conclude.

2 THEORETICAL FRAMEWORK

2.1 Derivation of the most unstable mode

The initial analytical formalism follows that of Jog & Solomon (1984a) for the two fluid approach, Romeo et al. (2010) concerning the inclusion of the turbulent motions of the gas, and Shadmehri & Khajenabi (2012) who combined both aspects. We recall here some of the basic assumptions. Both gas and stars in the disc are treated as isothermal fluids with velocity dispersions Σ_g and σ_* and their unperturbed surface densities are given by Σ_g and Σ_*, respectively. The scaleheights of the gaseous and stellar components are given by h_g and h_*, respectively. Starting from the perturbed and coupled hydrodynamical gas-stars equations, and a solution for the perturbed quantities that has the functional form $\exp\,[\mathrm{i}\,(\mathrm{kr} + \omega \mathrm{t})]$, Jog & Solomon (1984a) derived the dispersion relation that describes the growth rate of the instability in the linear regime, ω. This is given by the following biquadratic equation:

$$\omega^4 - \omega^2 \left(\alpha_* + \alpha_g\right) + \left(\alpha_* \alpha_g - \beta_* \beta_g\right) = 0, \tag{1}$$

where

$$\alpha_* = \kappa^2 + k^2 \sigma_*^2 - 2\pi G k \Sigma_* \frac{1}{1 + k h_*}, \tag{2}$$

$$\alpha_g = \kappa^2 + k^2 \Sigma_g^2 - 2\pi G k \Sigma_g \frac{1}{1 + k h_g}, \tag{3}$$

$$\beta_* = 2\pi G k \Sigma_* \frac{1}{1 + k h_*} \tag{4}$$

$$\beta_g = 2\pi G k \Sigma_g \frac{1}{1 + k h_g}, \tag{5}$$

[1] Keeping with the terminology used in Shi et al. 2011, we also use the term 'extended' to describe the dependence of the SFR on physical quantities pertaining to both gas and stars in galactic discs.

where κ is the epicyclic frequency, and $1/(1 + kh_{\rm g})$ and $1/(1 + kk_*)$ are the reduction factors due to the gas and stellar discs thickness, respectively (Vandervoort 1970; Romeo 1992). The solutions to equation (1) are given by

$$\omega^2(k) = \frac{1}{2}\left[\left(\alpha_* + \alpha_{\rm g}\right) \pm \sqrt{\left(\alpha_* + \alpha_{\rm g}\right)^2 - 4\left(\alpha_*\alpha_{\rm g} - \beta_*\beta_{\rm g}\right)}\right]. \tag{6}$$

Only one of these roots allows for unstable modes to grow. This is given by

$$\omega_-^2(k) = \frac{1}{2}\left[\left(\alpha_* + \alpha_{\rm g}\right) - \sqrt{\left(\alpha_* + \alpha_{\rm g}\right)^2 - 4\left(\alpha_*\alpha_{\rm g} - \beta_*\beta_{\rm g}\right)}\right]. \tag{7}$$

Inserting back the expressions of α_*, $\alpha_{\rm g}$, β_*, $\beta_{\rm g}$ from equations (2)–(5) into equation (7) and working in the limit where $h_*k \lesssim 1$ and $h_{\rm g}k \lesssim 1$, i.e. in the limit of the thin disc approximation in which case the perturbations have a length-scale that is of the order of, or larger than, the gaseous and stellar scalesheights, then equation (7) becomes

$$\omega_-^2(k) = \kappa^2 + \frac{\left(\sigma_*^2 + \Sigma_{\rm g}^2\right)}{2}k^2 - \pi G\left(\Sigma_* + \Sigma_{\rm g}\right)k$$
$$-\frac{k}{2}\left[\left(\sigma_*^2 - \Sigma_{\rm g}^2\right)^2 k^2 + 4\pi G\left(\sigma_*^2 - \Sigma_{\rm g}^2\right)\left(\Sigma_{\rm g} - \Sigma_*\right)k + 4\pi^2 G^2\left(\Sigma_* + \Sigma_{\rm g}\right)^2\right]^{1/2}, \tag{8}$$

which is independent of both h_* and $h_{\rm g}$. While this assumption is not explicitly necessary if $h_{\rm g}$ and h_* are known, the advantage of applying the thin disc approximation is that these two scales heights are generally poorly constrained for face-on disc galaxies. Under the plausible assumption that the gaseous component is turbulent, the surface density and velocity dispersion of the gas are scale dependent and are assumed to follow Larson type scaling relations (Larson 1981), and are given by

$$\Sigma_{\rm g} = \Sigma_{\rm g0}\left(\frac{k}{k_0}\right)^{-a}, \tag{9}$$

and

$$\Sigma_{\rm g} = \sigma_{\rm g0}\left(\frac{k}{k_0}\right)^{-b}, \tag{10}$$

where a and b are descriptive of the nature of turbulent motions, and $\Sigma_{\rm g0}$ and $v_{\rm g0}$ are the surface density and velocity dispersion on the scale of the spatial resolution of the observations (i.e. $2\pi/k_0$), respectively. Replacing equations (9)–(10) in equation (8) yields

$$\omega_-^2(k) = \kappa^2 + \frac{\sigma_*^2}{2}k^2 + \frac{\sigma_{\rm g0}^2}{2}\left(\frac{k}{k_0}\right)^{-2b}k^2 - \pi G\left(\Sigma_* + \Sigma_{\rm g0}\left(\frac{k}{k_0}\right)^{-a}\right)k$$
$$-\frac{k}{2}\left[\left(\sigma_*^2 - \sigma_{\rm g0}^2\left(\frac{k}{k_0}\right)^{-2b}\right)^2 k^2 + 4\pi G\left(\sigma_*^2 - \sigma_{\rm g0}^2\left(\frac{k}{k_0}\right)^{-2b}\right)\left(\Sigma_{\rm g0}\left(\frac{k}{k_0}\right)^{-a} - \Sigma_*\right)k\right.$$
$$\left. + 4\pi^2 G^2\left(\Sigma_* + \Sigma_{\rm g0}\left(\frac{k}{k_0}\right)^{-a}\right)^2\right]^{1/2}. \tag{11}$$

We posit that the fastest growing mode is directly linked to the SFR. The fastest growing mode, $k_{\rm SF}$, can be obtained by requiring that

$$\frac{{\rm d}\omega_-^2(k_{\rm SF})}{{\rm d}k} = 0, \tag{12}$$

which is an equation that can be solved numerically. It is interesting to note that equation (12) possesses always a positive, non-zero root, for any positive values of the exponents a and b when $a < 1/2$ and $b < 1/2$. These values are the typical upper limits measured for a and b in all phases of the interstellar gas. The full analytical expression of equation (12) is of little direct interest here and is given in Appendix A. It also implies that the SFR is independent of the galactic rotation (i.e. no dependence of κ). This is consistent with the findings of Dib et al. (2012), who found no correlation between the star formation levels in Galactic molecular clouds and the degree of shear the clouds are subjected to. Following the method of Dib et al. (2012), Thilliez et al. (2014) reached a similar conclusion for molecular clouds in the Large Magellanic Cloud. It is useful to point out that our definition of the characteristic length-scale of the most unstable mode ($\lambda_{\rm SF} = 2\pi/k_{\rm SF}$), which we associate with star formation, is different from the one used by Romeo & Falstad (2013; see also Fathi et al. 2015). The latter authors define the characteristic length-scale as being the scale at which the effective Toomre parameter drops below unity.

2.2 Connection to the SFR

The SFR can be directly related to the length-scale of the most unstable mode $\lambda_{\rm SF}$. The mass of the gas that is associated with $\lambda_{\rm SF}$ is given by

$$M_{\rm SF} = \bar{\rho} V_{\rm SF}, \tag{13}$$

where $\bar{\rho}$ is the average density within the mass $M_{\rm SF}$, and $V_{\rm SF}$ is the volume of the gravitationally unstable gas. In the limit of $k_{\rm SF}h_{\rm g} \lesssim 1$ as adopted above, $V_{\rm SF}$ is given by $V_{\rm SF} = \pi\lambda_{\rm SF}^2 2h_{\rm g}$ and the volume density of the gas can be replaced by the gas surface density. Thus, equation (13) becomes

$$M_{\rm SF} = \frac{\Sigma_{\rm g}}{2h_{\rm g}}\pi\lambda_{\rm SF}^2 2h_{\rm g} = \Sigma_{\rm g}\pi\lambda_{\rm SF}^2. \quad (14)$$

The theoretical SFR is then given by

$$\mathrm{SFR_{th}} \approx \epsilon_{\rm ff}\frac{M_{\rm SF}}{t_{\rm ff}}, \quad (15)$$

where $t_{\rm ff}$ is the free-fall time of the unstable mass reservoir, and $\epsilon_{\rm ff}$ is the efficiency of the star formation process per unit free-fall time. We approximate $t_{\rm ff}$ with $1/\sqrt{G\rho_{\rm mp0}}$, where $\rho_{\rm mp0}$ is the gas volume density at the mid-plane. The mid-plane volume density can be written as (e.g. Krumholz & McKee 2005)

$$\rho_{\rm mp0} \approx \frac{\pi G \phi_P \Sigma_{\rm g0}^2}{2\sigma_{\rm g0}^2}, \quad (16)$$

where $\Sigma_{\rm g0}$ and $\sigma_{\rm g0}$ carry the same meaning as in Section 2.1 and with ϕ_P being a term of order unity that describes the contribution of stars to the mid plane pressure. An approximation of ϕ_P is given by (e.g. Elmegreen 1989)

$$\phi_P \approx 1 + \frac{\Sigma_*}{\Sigma_{\rm g0}}\frac{\sigma_{\rm g0}}{\sigma_*}. \quad (17)$$

With these approximations, $t_{\rm ff}$ can be written as

$$t_{\rm ff} = \sqrt{\frac{2}{\pi}}\frac{1}{G}\frac{\sigma_{\rm g0}}{\Sigma_{\rm g0}}\left(1 + \frac{\Sigma_*}{\Sigma_{\rm g0}}\frac{\sigma_{\rm g0}}{\sigma_*}\right)^{-1/2}. \quad (18)$$

Combining equations (14) and (18) yields the expression for the $\mathrm{SFR_{th}}$:

$$\mathrm{SFR_{th}} = \epsilon_{\rm ff}\frac{\pi^{3/2}}{2^{1/2}}G\lambda_{\rm SF}^2\frac{\Sigma_{\rm g0}^2}{\sigma_{\rm g0}}\left(1 + \frac{\Sigma_*}{\Sigma_{\rm g0}}\frac{\sigma_{\rm g0}}{\sigma_*}\right)^{1/2}. \quad (19)$$

The theoretical estimate of the surface density of the SFR is then simply given by

$$\Sigma_{\rm SFR,th} = \frac{\mathrm{SFR_{th}}}{S}, \quad (20)$$

where S is the surface area covered by the beam size in the observations.

3 APPLICATION TO NGC 628

We test our model by comparing its predictions to the face-on, spiral galaxy NGC 628. The values of $\Sigma_{\rm H\,I}$ and $\sigma_{\rm H\,I}$ for NGC 628 are derived from the moment 0 and moment 2 maps of The H I Nearby Galaxy Survey (THINGS; Walter et al. 2008). The spatial resolution (i.e. beam size) for these observations at the distance of NGC 628 are 750 pc, thus, the surface area of the resolution element in NGC 628 used in this work is $S = 750 \times 750$ pc^2. As in Shi et al. (2011), the values of $\Sigma_{\rm H_2}$ are derived from the moment 0 CO $J = 1$–0 BIMA SONG survey (Helfer et al. 2003), and the stellar surface density is taken from the SIRTF Nearby Galaxies Survey (SINGS; Kennicutt et al. 2003). Since the H I gas is ubiquitously present in the galaxy, we approximate the velocity dispersion of the gas as being the velocity dispersion of the H I gas, $\Sigma_{\rm g} \approx \sigma_{\rm H\,I}$. Measurements of the stellar velocity dispersions in nearby galaxies are scarce. Yet, the VENGA survey has made such measurements, with selected mosaics, for a sample of nearby galaxies, including NGC 628 (Blanc et al. 2013). We use the same local observational estimates of $\Sigma_{\rm SFR}$ for NGC 628 (hereafter $\Sigma_{\rm SFR,obs}$) as in Shi et al. (2011), which are based on a combination of *GALEX* far-UV measurements (Gil de Paz, Boissier & Madore 2007) and *Spitzer* 24 μm (Kennicutt et al. 2003) and which have a 3σ lower limit of 10^{-4} M$_\odot$ yr^{-1} kpc^{-2}.

For each resolution element in NGC 628 with measurements in the VENGA survey, we estimate the value of $\lambda_{\rm SF}$ by solving equation (12). We then use equations (19) and (20) to evaluate the theoretical values of the SFR ($\mathrm{SFR_{th}}$) and the surface density of the SFR, $\Sigma_{\rm SFR,th}$. The number of resolution elements in NGC 628 that simultaneously have σ_* measurements in VENGA as well as measured values of $\Sigma_{\rm SFR,obs}$ is 91. Fig. 1 displays the distribution function of $\lambda_{\rm SF}$ for these pointings, obtained for $a = b = 1/3$. The values of $a = 1/3$ and $b = 1/3$ are consistent with average values of these quantities derived using cold H I intensity fluctuations (Lazarian & Pogosyan 2000; Elmegreen, Kim & Staveley-Smith 2001; Begum, Chengalur & Bhardwaj 2006; Dutta et al. 2009). The distribution in Fig. 1 peaks at ≈850 pc and is positively skewed towards larger values, and we argue in Appendix B that this result is not dependent on the spatial resolution of the observations. While there are no accurate estimates of the vertical scales heights of gas and stars in NGC 628,[2] the values of $\lambda_{\rm SF}$ are large enough such that the

[2] Kregel, van der Kruit & de Grijs (2002) argued that there is a constant ratio of the radial to vertical length-scales in galactic discs of $l_*/h_* \approx, 7.3 \pm 2.2$. With the measured value of $l_* \approx 2.3$ kpc in NGC 628 (Leroy et al. 2008), this yields a value of $h_* \approx 315$ pc, under the assumption that h_* is independent of galactic radius. From an analysis of the H I line power spectrum, Dutta et al. (2008) argued for an upper limit on the H I gas vertical scales height of 800 pc.

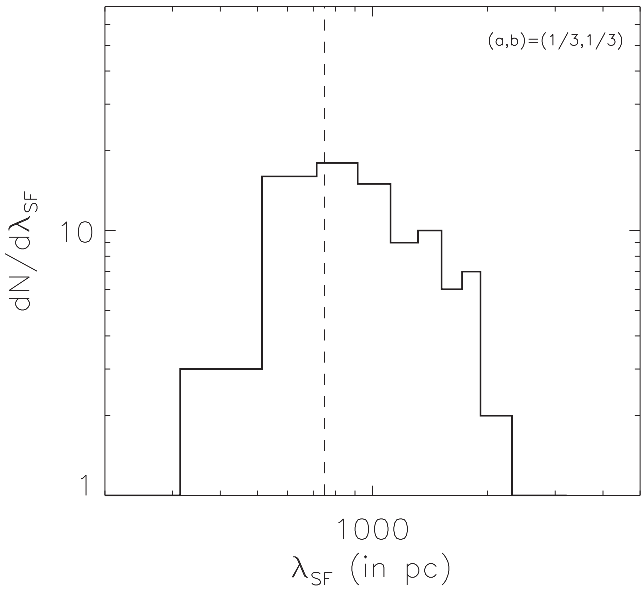

Figure 1. Distribution function of the wavelength of the most unstable mode λ_{SF} for the sample of data points that are used in this study (see text for the selection criteria) and for values of $a = 1/3$ and $b = 1/3$. The spatial resolution of the observations ($\lambda_0 = 750$ pc) is shown with the dashed line.

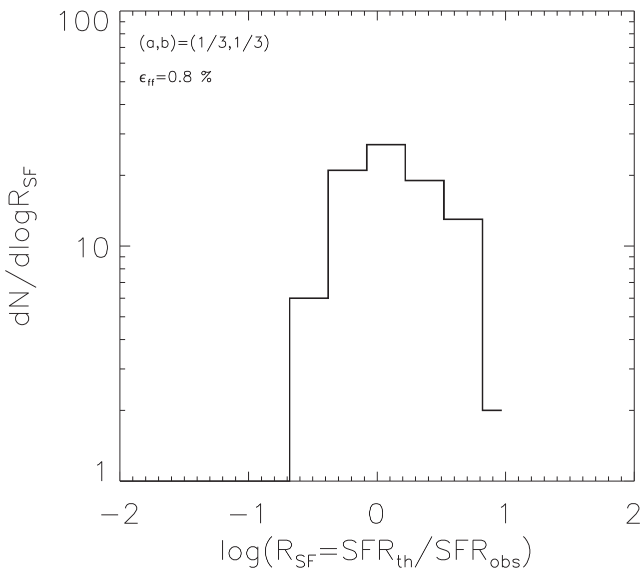

Figure 2. Distribution function of the ratio of the theoretical estimate of the SFR (SFR_{th}) to the observed one (SFR_{obs}) for the sample of data points that are used in this study (see text for the selection criteria) and for values of $a = 1/3$, $b = 1/3$ and $\epsilon_{ff} = 0.8$ per cent.

condition $\lambda_{SF} \gtrsim 2\pi h_g$ and $\lambda_{SF} \gtrsim 2\pi h_*$ seems to be reasonably fulfilled for almost all resolution elements. The values of SFR_{th} and $\Sigma_{SFR,th}$ are then derived following the formalism given in Section 2.2 with an assigned value of $\epsilon_{ff} = 0.008$. A value of 0.008 for ϵ_{ff} is consistent with the Galaxy-wide average value of ≈0.006 (Krumholz & Tan 2007; Murray 2011), and with the average value of $\epsilon_{ff} \approx 0.01$ found in numerical simulations (e.g. Semenov, Kravtsov & Gnedin 2016, see fig. 2 in their paper). This value is a factor ≈10 smaller than the average value measured on the scale of GMCs in the Galaxy (Murray 2011). This is expected since the gas is denser and more gravitationally bound in GMCs than the spatially averaged gas densities on scales of 750 pc (as are the observations of NGC 628) or on entire galactic scales.

Fig. 2 displays the distribution function of the ratio of the theoretical to observational SFRs (SFR_{th}/SFR_{obs}). The dispersion in this distribution is ≈0.3 dex. Fig. 3 displays the scatter plots in the $\Sigma_g - \Sigma_{SFR}$ space (left-hand column) and in the $\Sigma_* - \Sigma_{SFR}$ space (right-hand column). The observations are shown with the red open triangles, and the theoretical estimates are shown with the black open diamonds (top) and as a closed contours containing 68 per cent of the theoretical points (bottom). A noticeable aspect of Fig. 3 is that in the low surface density regime ($\Sigma_g \lesssim$ 10–15 $M_\odot$ pc^{-2}), the model matches perfectly the data, both in terms of the dependence of Σ_{SFR} on Σ_g and Σ_* and in terms of the level of dispersion at any given value of Σ_g and Σ_*. At higher surface densities ($\Sigma_g \gtrsim 15$ $M_\odot$ pc^{-2}), the theoretical estimates of Σ_{SFR} are larger than the observed ones by factors of ≈2–5. It is important to note that our formalism does not account explicitly for the effects of feedback from massive stars, which are more important at higher surface densities where more massive clusters can form. The

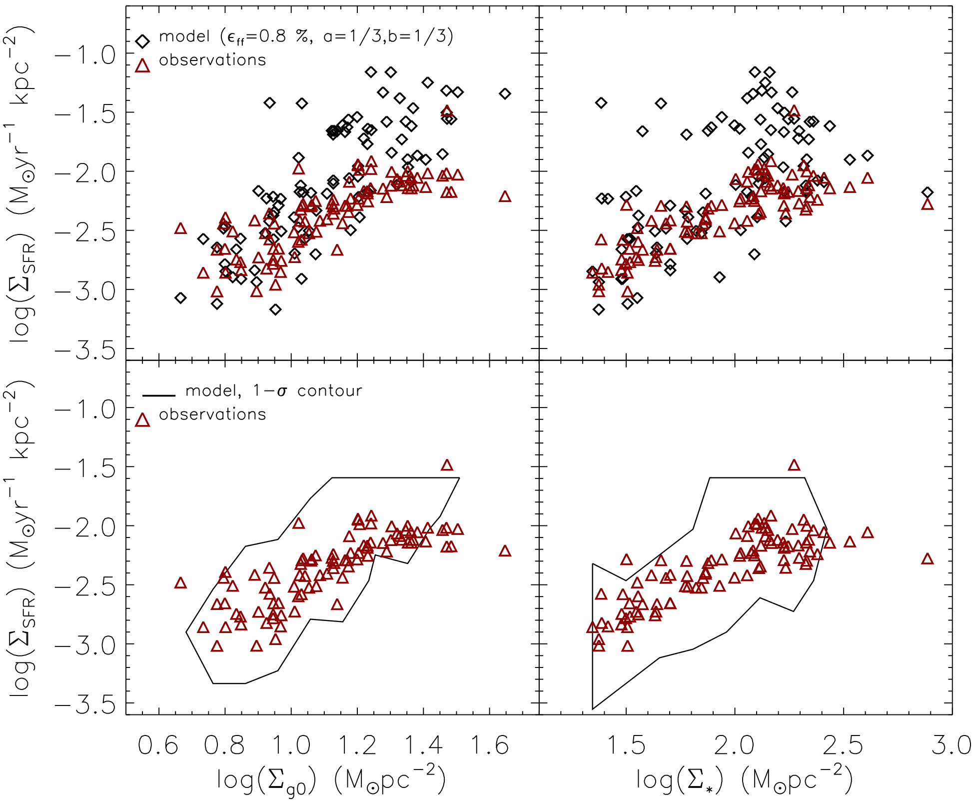

Figure 3. The surface density of the SFR plotted as a function of the total gas surface density (left-hand panels) and stellar surface density (right-hand panels). The observational data are shown with the red open triangles. The theoretical estimates from the model are shown with the open black diamonds (top panels), and as a closed contour containing 68 per cent of the estimates (bottom panels). The free parameters of the model are taken to be $a = b = 1/3$ and $\epsilon_{ff} = 0.8$ per cent. Here, Σ_{g0} is the total surface density of the gas measured on a spatial scale, which is equal to the spatial resolution of the observations (i.e. 750 pc).

increased effect of feedback at high surface densities leads to a more rapid expulsion of the gas from the clusters and to a reduction of the star formation efficiency per unit time (Dib 2011a). Dib (2011a), showed that in the surface density regime relevant for this work ($1\ M_\odot\ pc^{-2} \lesssim \Sigma_g \lesssim 50\ M_\odot\ pc^{-2}$), the value of the star formation efficiency per free-fall time (ϵ_{ff}) decreases by a factor of ≈4 going from low to higher gas surface densities, and this is valid for any given value of the gas phase metallicity. Using a scaling of ϵ_{ff} as a function of Σ_g ($\epsilon_{ff} \propto \Sigma_g^{-0.34}$) (Dib 2011a), and fixing the value of $\epsilon_{ff} = 0.008$ at $\Sigma_g = 1\ M_\odot\ yr^{-1}$, we make a new estimate of $\Sigma_{SFR,th}$. The distribution function of the ratio SFR_{th}/SFR_{obs} in the presence of the effects of feedback is displayed in Fig. 4. While the distribution in Fig. 4 does not peak at unity (because of the arbitrary choice of fixing $\epsilon_{ff} = 0.008$ at $\Sigma_g = 1\ M_\odot\ yr^{-1}$), the inclusion of a correction due to feedback removes the positive skewness of the distribution (i.e. at high surface densities) and leads to a quasi-symmetric dispersion around each side of the observations. Fig. 5 displays the corresponding scatter plots for Σ_{SFR} versus Σ_g and Σ_* (left- and right-hand panels, respectively). The figure shows that the inclusion of feedback in the treatment of GI in a star+gas galactic disc is necessary in order to better match the observed dependence of Σ_{SFR} on both Σ_g and Σ_*.

4 CONCLUSIONS

In this work, we explore the dependence of the surface density of star formation in galactic discs on the gas and stellar surface densities and velocity dispersions. We treat both gas and stars as an isothermal fluid and use the linear stability analysis of the gravitationally coupled hydrodynamical equations in order to derive the wavelength of the most unstable mode of the GI (λ_{SF}). We find that the latter quantity is a function of the stellar surface density, the gas surface density, the velocity dispersion of stars and the scaling laws of turbulence in the gas phase. When applying our model to the face-on, spiral galaxy NGC 628, for which all the required observational data are available, we find that the distribution of λ_{SF} for the ensemble of resolution elements for which the required stellar+gas data is available peaks at ≈850 pc and is skewed towards higher values (with a tail of the distribution up to ≈2.5 kpc; see Fig. 1). GIs on such large scales are likely to determine the rate of GMC formation. In turn, stars form in GMCs with a distribution of the star formation efficiencies that depend on the distribution of GMC masses, and on the distributions of their internal physical and dynamical properties coupled to a regulation provided by stellar feedback (e.g. Padoan & Nordlund 2011; Dib et al. 2013). It is therefore reasonable to assume that reservoirs of gas that become gravitationally unstable on large scales are correlated with the SFR on these scales. For a given set of physical conditions in each resolution elements of NGC 628, we derive the theoretical value of the SFR under the assumption that the fastest growing mode of the gas+star GI is directly linked to the

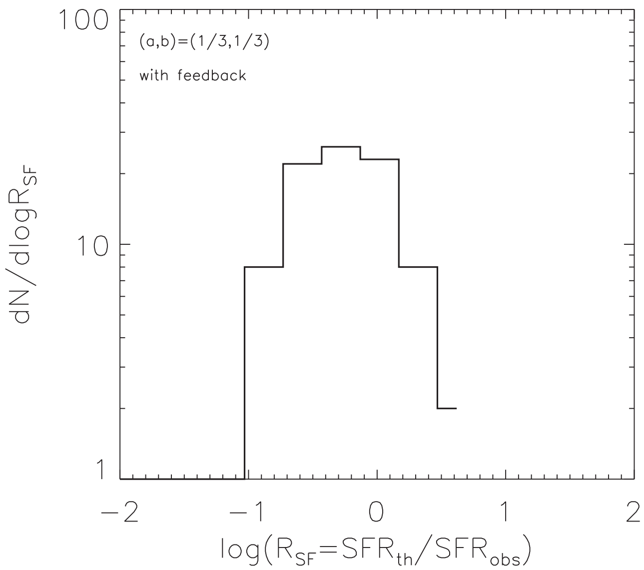

Figure 4. Similar to Fig. 2, but in this case, the efficiency of star formation per unit free-fall time is taken to depend on the gas surface density following $\epsilon_{ff} \propto \Sigma_g^{-0.34}$ and normalized to be 0.8 per cent at $\Sigma_g = 1\ M_\odot\ pc^{-2}$.

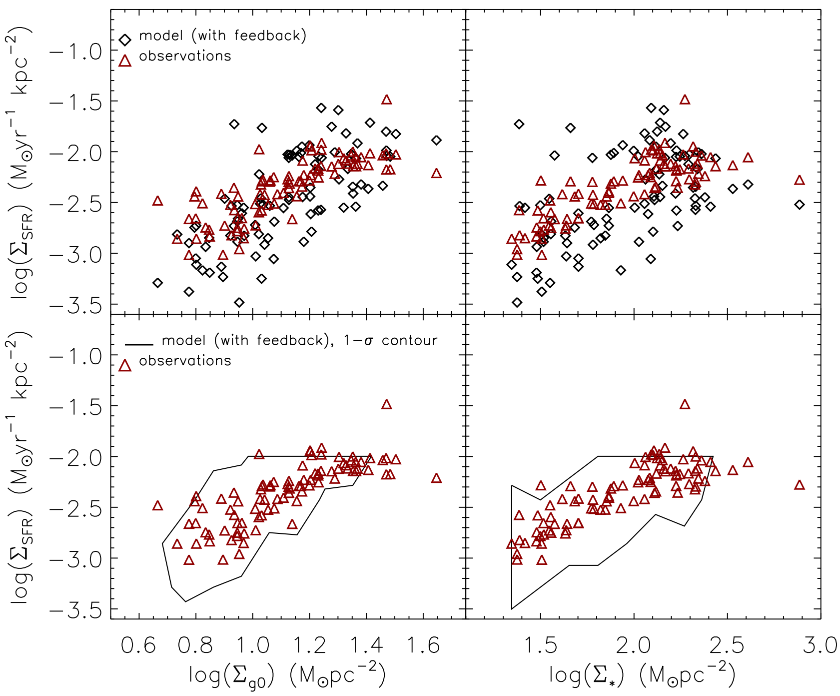

Figure 5. Similar to Fig. 3, but in this case, the efficiency of star formation per unit free-fall time is taken to depend on the gas surface density following $\epsilon_{ff} \propto \Sigma_g^{-0.34}$ and normalized to be 0.8 per cent at $\Sigma_g = 1\ M_\odot\ pc^{-2}$. Here, Σ_{g0} is the total surface density of the gas measured on a spatial scale, which is equal to the spatial resolution of the observations (i.e. 750 pc).

SFR. The theoretical surface density of the SFR ($\Sigma_{SFR,th}$) is obtained by dividing the SFR by the physical surface area of the surface element in the observations. The only free parameters of the models are the exponents of the turbulence scaling laws of the gas (i.e. *a*, and *b* which are the exponents of the gas surface density and velocity dispersion size relations, see equations 10 and 11) and the star formation efficiency per unit free-fall time, ϵ_{ff}. The values of *a* and *b*, and ϵ_{ff} are fixed at $a = b = 1/3$ and $\epsilon_{ff} = 0.8$ per cent, respectively. These values of *a* and *b* are appropriate for the description of the structure and velocity dispersion of the cold neutral hydrogen in the disc galaxies. A fixed value of ϵ_{ff} serves only as a normalization, and does not affect neither the shapes of the Σ_g–Σ_{SFR} and Σ_*–Σ_{SFR} relations, nor the amount of scatter at any fixed value of Σ_g or Σ_*.

We find an encouraging match between the theoretical estimates of the surface density of star formation $\Sigma_{SFR,th}$ from our model and the observational values for NGC 628 ($\Sigma_{SFR,obs}$), both in terms of the shapes of the Σ_g–Σ_{SFR} and Σ_*–Σ_{SFR} scatter relations and in terms of the dispersion of the data points at fixed values of Σ_g or Σ_*. The model-observations matching is further improved if the value of ϵ_{ff} is taken to decrease with increasing gas surface density as earlier suggested by Dib (2011a,b). The origin of the dependence of ϵ_{ff} on Σ_g is attributed to the effects of feedback in the pre-supernova phase in stellar clusters. More massive clusters are more likely to form at higher surface densities. Gas expulsion from more massive clusters occurs on shorter time-scales than in lower mass clusters (Dib et al. 2013), and the rapid expulsion of gas results in a faster quenching of star formation and to a reduction of the star formation efficiency per unit time. Our model opens a new path towards a better understanding of the dependence of the SFR in galaxies on the local stellar and gas properties. Higher spatial and spectral resolution observations will allow us to further constrain the model and will also help reduce the number of free parameters by directly measuring the scaling laws of turbulence.

ACKNOWLEDGEMENTS

We thank the referee Alessandro Romeo for a careful reading of the paper which helped clarify some aspects of the text, Sophia Lianou and Matthew Orr for useful comments on a draft version of this paper and Shi Yong for sharing some of the observational data. SD acknowledges the support provided by a Marie Curie Intra European Fellowship under the European Community's Seventh Framework Program FP7/2007-2013 grant agreement no 627008, during the early phase of this work. SH acknowledges financial support from DFG program HO 5475/2-1. GB is supported by CONICYT/FONDECYT programa de iniciación Folio 11150220. This research has made use of NASA's Astrophysics Data System Bibliographic Services.

REFERENCES

Begum A., Chengalur J. N., Bhardwaj S., 2006, MNRAS, 372, L33
Bigiel F., Leroy A., Walter F., Brinks E., de Blok W. J. G., Madore B., Thornley M. D., 2008, AJ, 136, 2846
Blanc G. A., Heiderman A., Gebhardt K., Evans N. J. II, Adams J., 2009, ApJ, 704, 842
Blanc G. A. et al., 2013, ApJ, 145, 138
Blitz L., Rosolowsky E., 2006, ApJ, 650, 933
Dib S., 2011a, ApJ, 737, L20
Dib S., 2011b, in Alvaro Navarro E. J., Gallego Calvente A. T., Zapatero Osorio M. R., eds, Stellar Clusters & Associations: A RIA Workshop on Gaia. p. 30
Dib S., Piau L., Mohanty S., Braine J., 2011a, MNRAS, 415, 3439
Dib S., Piau L., Mohanty S., Braine J., 2011b, in Alicia G., Belkacem K., Samadi R., Valls-Gabaud D., eds, SF2A-2011, Proceedings of the Annual meeting of the French Society of Astronomy and Astrophysics, (Paris: Societe Francaise dAstronomie et dAstrophysique), p. 275
Dib S., Helou G., Moore T. J. T., Urquhart J. S., Dariush A., 2012, ApJ, 758, 125
Dib S., Gutkin J., Brandner W., Basu S., 2013, MNRAS, 415, 3727
Dopita M. A., 1985, ApJ, 295, L5
Dopita M. A., Ryder S. D., 1994, ApJ, 430, 163
Dutta P., Begum A., Bharadwaj S., Chengalur J. N., 2008, MNRAS, 384, 34
Dutta P., Begum A., Bharadwaj S., Chengalur J. N., 2009, MNRAS, 398, 887
Elmegreen B. G., 1989, ApJ, 338, 178
Elmegreen B. G., Kim S., Staveley-Smith L., 2001, ApJ, 548, 749
Escala A., 2011, ApJ, 735, 56
Fathi K. et al., 2015, 806, L34
Federrath C., 2013, MNRAS, 436, 316
Gao Y., Solomon P. M., 2004, ApJ, 606, 271
Gil de Paz A., Boissier S., Madore B. F., 2007, ApJS, 173, 185
Helfer T. T., Thornley M. D., Regan M. W., Wong T., Sheth K., Vogel S. N., Blitz L., Bock D. C.-J., 2003, ApJS, 145, 259
Hennebelle P., Chabrier G., 2011, ApJ, 743, 29
Hoffman V., Romeo A. B., 2012, MNRAS, 425, 1511
Jog C. J., Solomon P. M., 1984a, ApJ, 276, 114
Jog C. J., Solomon P. M., 1984b, ApJ, 276, 127
Kennicutt R. C. Jr., 1998, ApJ, 498, 541
Kennicutt R. C. et al., 2003, PASP, 115, 928
Kraljic K., Renaud F., Bournaud F., Combes F., Elmegreen B., Emsellem E., Teyssier R., 2014, ApJ, 784, 112
Kregel M., van der Kruit P. C., de Grijs R., 2002, MNRAS, 334, 646
Krumholz M. R., McKee C. F., 2005, ApJ, 630, 250
Krumholz M. R., Tan J. C., 2007, ApJ, 654, 304
Larson R. B., 1981, MNRAS, 194, 809
Lazarian A., Pogosyan D., 2000, ApJ, 537, 720
Leroy A. K., Walter F., Brinks E., Bigiel F., de Blok W. J. G., Madore B., Thornley M. D., 2008, ApJ, 136, 2782
Liu T. et al., 2016, ApJ, 829, 59
Madore B. F., 1977, MNRAS, 178, 1
Meidt S. et al., 2013, ApJ, 779, 45
Murray N., 2011, ApJ, 729, 133
Orr M. E. et al., 2017, MNRAS, preprint (arXiv:1701.01788)
Padoan P., Nordlund Å., 2011, ApJ, 730, 40
Press W. H., Teukolsky S. A., Vetterling W. T., Flannery B. P., 1992, Numerical Recipes in C. The Art of Scientific Computing. Cambridge Univ. Press
Rafikov R. R., 2001, MNRAS, 323, 445
Rahmani S., Lianou S., Barmby P., 2016, MNRAS, 456, 4128

Renaud F., Kraljic K., Bournaud F., 2012, ApJ, 760, 16
Romeo A. B., 1992, MNRAS, 256, 307
Romeo A. B., Agertz O., 2014, MNRAS, 442, 1230
Romeo A. B., Falstad N., 2013, MNRAS, 433, 1389
Romeo A. B., Wiegert J., 2011, MNRAS, 416, 1191
Romeo A. B., Burkert A., Agertz O., 2010, MNRAS, 407, 1223
Schmidt M., 1959, ApJ, 129, 243
Semenov V. A., Kravtsov A. V., Gnedin N. Y., 2016, ApJ, 826, 200
Shadmehri M., Khajenabi F., 2012, MNRAS, 421, 841
Shetty R., Kelly B. C., Bigiel F., 2013, MNRAS, 430, 188
Shi Y., Helou G., Yan L., Wu Y., Papovich C., Stierwalt S., 2011, ApJ, 733, 87
Tassis K., 2007, MNRAS, 382, 1317
Thilliez E., Maddison S. T., Hughes A., Wong T., 2014, PASA, 31, 3
Toomre A., 1964, ApJ, 139, 1217
Vandervoort P. O., 1970, ApJ, 161, 87
Wada K., Norman C. A., 2007, ApJ, 660, 276
Walter F., Brinks E., de Block W. J. G., Bigiel F., Kennicutt R. C. Jr., Thornley M. D., Leroy A., 2008, AJ, 136, 2563
Westfall K. B., Andersen D. R., Bershady M. A., Martinsson T. P. K., Swaters R. A., Verheijen M. A. W., 2014, ApJ, 785, 43
Wong T., Blitz L., 2002, ApJ, 569, 157

APPENDIX A: GOVERNING EQUATION FOR $k_{\rm SF}$

The derivation of the wavenumber of the fastest growing mode of the instability, $k_{\rm SF}$, is achieved using equation (12), where ω_-^2 is given by equation (11). There exist an analytical expression for the general equation of $k_{\rm SF,}$ which is given by

$$\begin{aligned}
&\sigma_*^2 k_{\rm SF} + \sigma_{\rm g0}^2(1-b)\left(\frac{1}{k_0}\right)^{-2b} k_{\rm SF}^{1-2b} - \pi G\Sigma_* - \pi G\Sigma_{\rm g0}\left(\frac{k_{\rm SF}}{k_0}\right)^{-a} \\
&-\left[\left(\sigma_*^2 - \sigma_{\rm g0}^2\left(\frac{k_{\rm SF}}{k_0}\right)^{-2b}\right)^2 k_{\rm SF}^2 + 4\pi G\left(\Sigma_{\rm g0}\left(\frac{k_{\rm SF}}{k_0}\right)^{-a} - \Sigma_*\right)\left(\sigma_*^2 - \sigma_{\rm g0}^2\left(\frac{k_{\rm SF}}{k_0}\right)^{-2b}\right)k_{\rm SF}\right. \\
&\left.+4\pi^2 G^2\left(\Sigma_{\rm g0}\left(\frac{k_{\rm SF}}{k_0}\right)^{-a} + \Sigma_*\right)^2\right]^{1/2} \\
&-k_{\rm SF}\frac{\left[2k_{\rm SF}\left(\sigma_*^2 - \sigma_{\rm g0}^2\left(\frac{k_{\rm SF}}{k_0}\right)^{-2b}\right)^2 + 4b\sigma_{\rm g0}^2\left(\frac{k_{\rm SF}}{k_0}\right)^{-2b} k_{\rm SF}\left(\sigma_*^2 - \sigma_{\rm g0}^2\left(\frac{k_{\rm SF}}{k_0}\right)^{-2b}\right)\right]}{D} \\
&+k_{\rm SF}\frac{\left[4\pi G\left(\Sigma_{\rm g0}\left(\frac{k_{\rm SF}}{k_0}\right)^{-a} - \Sigma_*\right)\left(\sigma_*^2 - \sigma_{\rm g0}^2\left(\frac{k_{\rm SF}}{k_0}\right)^{-2b}\right) - 4\pi a G\Sigma_{\rm g0}\left(\frac{k_{\rm SF}}{k_0}\right)^{-a}\left(\sigma_*^2 - \sigma_{\rm g0}^2\left(\frac{k_{\rm SF}}{k_0}\right)^{-2b}\right)\right]}{D} \\
&+k_{\rm SF}\frac{\left[8a\pi^2 G^2\Sigma_{\rm g0}\left(\frac{k_{\rm SF}}{k_0}\right)^{-a} k_{\rm SF}^{-1}\left(\Sigma_{\rm g0}\left(\frac{k_{\rm SF}}{k_0}\right)^{-a} + \Sigma_*\right) + 8\pi b G\sigma_{\rm g0}^2\left(\frac{k_{\rm SF}}{k_0}\right)^{-2b}\left(\Sigma_{\rm g0}\left(\frac{k_{\rm SF}}{k_0}\right)^{-a} - \Sigma_*\right)\right]}{D} \\
&= 0
\end{aligned} \tag{A1}$$

with

$$\begin{aligned}
D = 4&\left[k_{\rm SF}^2\left(\sigma_*^2 - \sigma_{\rm g0}^2\left(\frac{k_{\rm SF}}{k_0}\right)^{-2b}\right)^2 + 4\pi G k_{\rm SF}\left(\Sigma_{\rm g0}\left(\frac{k_{\rm SF}}{k_0}\right)^{-a} - \Sigma_*\right)\left(\sigma_*^2 - \sigma_{\rm g0}^2\left(\frac{k_{\rm SF}}{k_0}\right)^{-2b}\right)\right. \\
&\left.+4\pi^2 G^2\left(\Sigma_{\rm g0}\left(\frac{k_{\rm SF}}{k_0}\right)^{-a} - \Sigma_*\right)^2\right]^{1/2}.
\end{aligned} \tag{A2}$$

Given the values of $k_0 = 2\pi/\lambda_0$, where λ_0 is the physical size of the resolution element in the observations. For each resolution element of the NGC 628 galaxy, we solve equation (A1) numerically using a globally convergent Broyden's method (Press et al. 1992)

APPENDIX B: DO THE RESULTS DEPEND ON THE SPATIAL RESOLUTION OF THE OBSERVATIONS ?

The question may arise whether the solutions obtained for $\lambda_{\rm SF}$ using equation (12) (i.e. equation A1 in its detailed form) depend on the spatial resolution of the observations (here $\lambda_0 = 750$ pc). It should be noted that the surface density and velocity dispersion of the gas have a scale dependance on the dimensionless number k/k_0 (and not merely on k_0). None the less, we test this by performing the following simple test. We assume that the observations have been performed on a spatial resolution of 375 pc (thus k_0 is now replaced by $2k_0$, where k_0 is the wavenumber

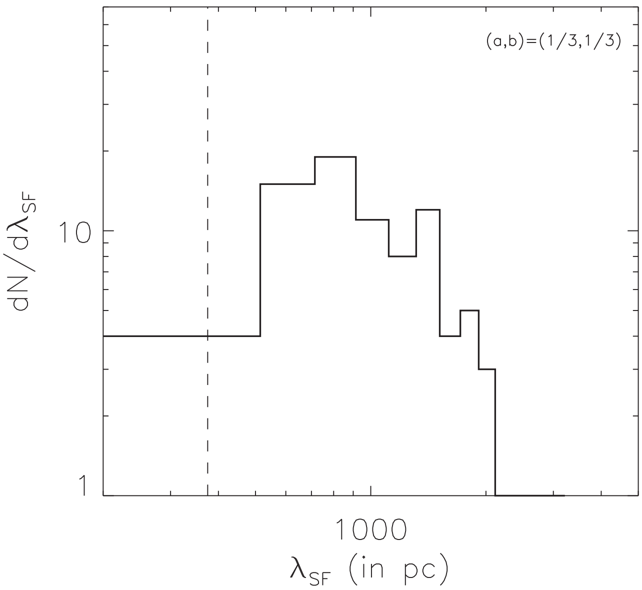

Figure B1. Same as Fig. 1 but for an adjusted spatial resolution in the observation of 375 pc (shown as the dashed line). The values of the parameters are kept at $a = 1/3$ and $b = 1/3$.

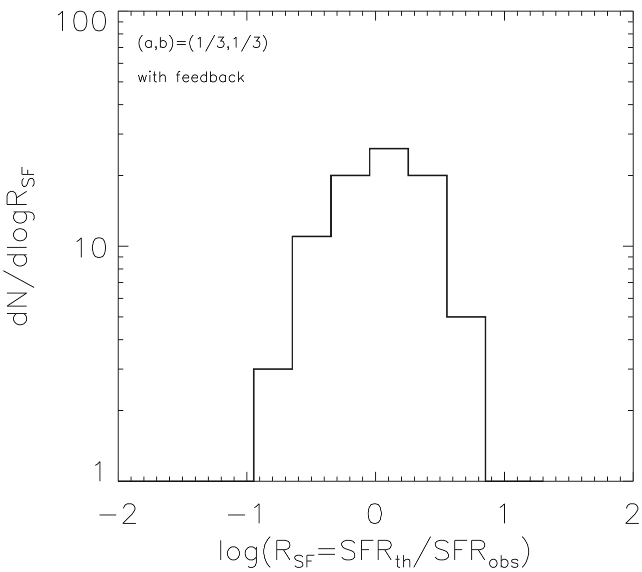

Figure B2. Similar to Fig. 4, but in this case, we assume a spatial resolution of 375 pc (marked in the figure by the dashed line). The stellar surface density and velocity dispersion are kept to their similar value for the resolution of 750 pc, and the surface density and velocity dispersion of the gas are adapted using equations (10) and (11), respectively.

associated with the original spatial resolution of 750 pc). We do not possess observations that have been obtained self-consistently at a spatial resolution that is half of the spatial resolution of the observations at hand. However, we adapt the current observations to present those that could be obtained with an improved spatial resolution by a factor 2. In the absence of a better guess, the stellar surface density and velocity dispersion for the resolution $\lambda_0/2$ are kept the same as on the scale λ_0. The velocity dispersion and surface density of the gas in equations (10) and (11) have to be multiplied by the factors $2^{-\beta}$ and $2^{-\alpha}$, respectively. For $\alpha = \beta = 1/3$, the gas velocity dispersion and surface density are both reduced by a factor $2^{-1/3}$. These assumptions generate only approximate conditions for the stellar and gas components in each constructed half-resolution element as one expects that there would be local fluctuations of the stellar velocity and surface density on smaller scales.

Fig. B1 displays the distribution of the wavelengths of the most unstable mode (λ_{SF}) with the new adopted spatial resolution. As expected, the choice of a different spatial resolution (here a higher resolution) does not affect the results and the distribution of λ_{SF} still peaks at ≈850–900 pc. For this same adopted spatial resolution, Fig. B2 displays the ratio of the theoretical to observed SFRs, while Fig. B3 displays the surface density of the SFR as a function of the surface density of the gas (left-hand panels) and of the stars (right-hand panels;

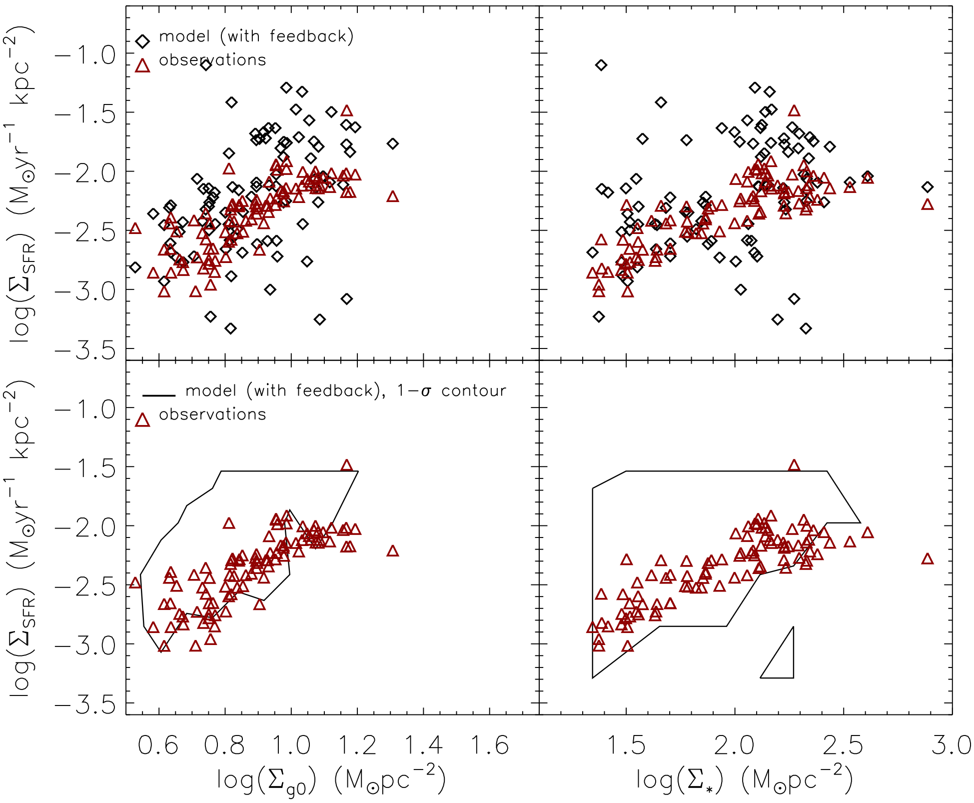

Figure B3. Similar to Fig. 5, but in this case, we assume a spatial resolution of 375 pc. The stellar surface density and velocity dispersion are kept to their similar value for the resolution of 750 pc, and the surface density and velocity dispersion of the gas are adapted using equations (10) and (11), respectively. Here, Σ_{g0} is the total surface density of the gas measured on a spatial scale, which is equal to the adjusted spatial resolution of the observations (here 375 pc).

for the model as a scatter plot in the top panels and as a closed 1σ contour in the bottom panels). In this case, the efficiency of star formation per free-fall time ϵ_{ff} has been taken to include a correction for feedback (i.e. as in Figs 4 and 5). The existence of more outliers that result in a larger scatter is probably due to the approximations made in constructing the physical quantities (especially Σ_* and σ_*) for the higher spatial resolution case.

This paper has been typeset from a TEX/LATEX file prepared by the author.